

## SIDELobe SUPPRESSED BEAM-PATTERNS OF A COAXIAL CIRCULAR ARRAY AT OPERATING WAVELENGTHS USEFUL TO UNDERWATER TRANSDUCER APPLICATIONS

Bishwajit Chakraborty

National Institute of Oceanography, Dona Paula, Goa 403 004, India.

### Abstract

*This analysis presents an improved beam-pattern for a coaxial circular array, using Taylor's shading approximations. Element excitation coefficients are also presented for 24 elements, for different wavelengths. A comparison of the noise improvement figures is done for different operating wavelengths to ensure wide applicability of such an array for underwater transducer applications.*

### Introduction

A well-resolved symmetrical and narrow beam is not an unknown feature of circular arrays. Apart from this, structures whose geometries depend upon dimensionless parameters (e.g. angles for circles), would show the property of frequency scaling [1]. An earlier study [2] with respect to the far-field pattern and field frequency responses of a coaxial circular array for underwater applications revealed that the main beamwidth was remarkably low at operating wavelengths  $0.5\lambda$ ,  $1.0\lambda$  and  $1.5\lambda$ , where  $\lambda$  is the design wavelength. It was also observed that the presence of higher side-lobe levels would create more difficulties in the easy operation of the system. An application of a suitable shading technique was found to be effective in reducing side-lobes down to a desired level ( $-20\text{dB}$ ). The power pattern of a coaxial circular array of uniformly excited circular plate elements for unsuppressed side-lobes is presented in Figure 2.

Taylor's shading approximation [3, 4] is often used as a basis for the suppression of the beam-pattern of a circular array. In the present study, the above technique is employed in a coaxial circular array of three turns to give a suppressed side-lobe level ( $-20\text{dB}$  relative to the beam-pattern of a uniformly excited array), maintaining the same main beamwidth. The excitation coefficients for each element are obtained by means of inverse techniques for different operating wavelengths (Table 2).

In addition, comparison of a noise improvement figure for the spherical noise model is also carried out, considering each radiator as a point source, for a discrete circular plate (unshaded pattern) as well as for circular plates of shaded pattern ( $-20\text{dB}$  of side-lobe level).

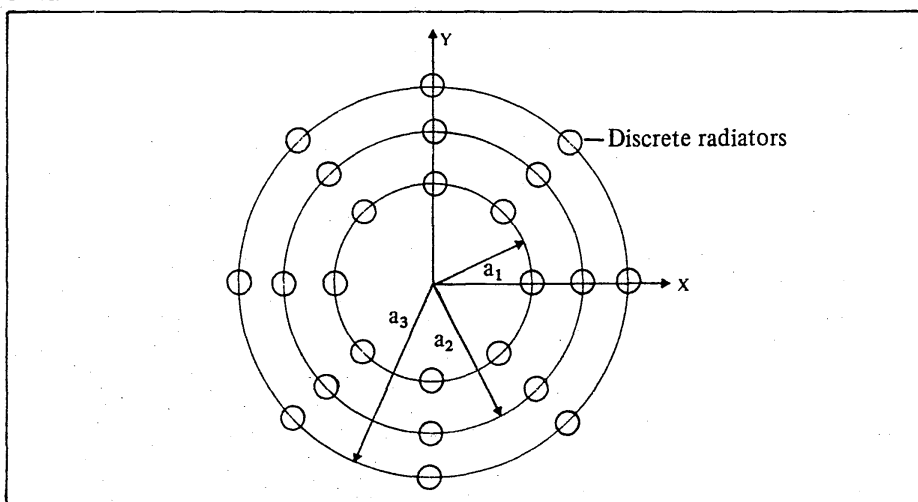


Figure 1. Coaxial circular array geometry.

## Analysis

Figure 1 shows three circles of different radii on the  $xy$ -plane. Each circle consists of eight elements, and a total of 24 elements are distributed in an array system. The far-field pattern for such an array is given by [2]

$$F(\theta, \phi) = \sum_{m=1}^8 \exp j\beta a_1 \sin\theta \cos\phi \cos(m-1)\pi/4 + a_1 \sin\theta \sin\phi \sin(m-1)\pi/4 + \\ + \sum_{m=9}^{16} \exp j\beta a_2 \sin\theta \cos\phi \cos(m-1)\pi/4 + a_2 \sin\theta \sin\phi \sin(m-1)\pi/4 + \\ + \sum_{m=17}^{24} \exp j\beta a_3 \sin\theta \cos\phi \cos(m-1)\pi/4 + a_3 \sin\theta \sin\phi \sin(m-1)\pi/4$$

. Element Pattern (1)

Here,  $m$  is the radiator number;  $a_1$ ,  $a_2$  and  $a_3$ , are the radii of the inner, middle and outermost radii of the circles (in the present case  $a_1 = 4.0\lambda$ ,  $a_2 = 6.0\lambda$  and  $a_3 = 8.0\lambda$ ).  $\beta$  is the wave number ( $= 2\pi/\lambda_0$ ) and  $\lambda_0$  is the operating wavelength.

In order to suppress the  $\bar{p}-1$  side-lobes of eqn.1, to achieve the desired level for inside lobes while keeping the same main beam width, the new pattern can be presented as

$$F'(u) = F(u) \prod_{p=1}^{\bar{p}-1} (1 - u^2/u_p^2) / \sum_{p=1}^{\bar{p}} (1 - u^2/r_{1p}^2), \quad (2)$$

where

$$u_p = r_{1\bar{p}}^2 (A^2 + (p-0.5)^2) / (A^2 + (\bar{p}-0.5)^2)$$

(known as the new positions of the side-lobes, they are similar in the present analysis),

and

$$A = 1/\pi \cosh^{-1} 10 \text{ (reqd. side-lobe level)/20}$$

$F(u)$  is the corresponding value of  $u$  from the array factor for a uniformly excited element,  $u = 2a_3 \sin\theta$ , where  $a_3$  is the radius of the outermost circle ( $8.0\lambda$  in the present case) and  $\theta$  is the vertical and  $\phi (= 0^\circ)$  is the azimuthal angle.  $\bar{p}$  is the number of iterations chosen from the array pattern of figure 2 (i.e., number of intervening side-lobes to be suppressed) and  $p$  is a factor varying from 1 to  $\bar{p}-1$ .  $r_{1p} = 2a \sin\theta_p$ , is obtained from figure 2 for the different points of nulls, and  $r_{1\bar{p}}$  is equal to  $2a \sin\theta_{\bar{p}}$ , the last null angle up to which suppression is to be carried out.

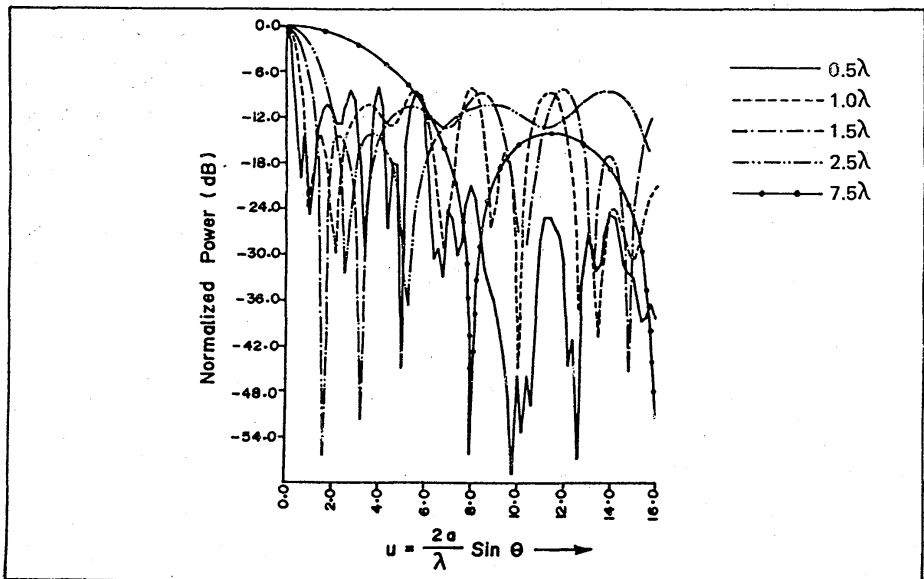


Figure 2. Vertical power pattern in the  $\phi = 0^\circ$  plane for unshaded array elements at different operating wavelengths.

Table 1  
Selected values of  $\bar{p}$  (number of iterations) for  $-20\text{dB}$  side-lobe levels at different operating wavelengths.

	Operating wavelengths $\lambda$	Selected $\bar{p}$
1	0.5	11
2	1.0	8
3	1.5	6
4	2.5	2
5	7.5	2

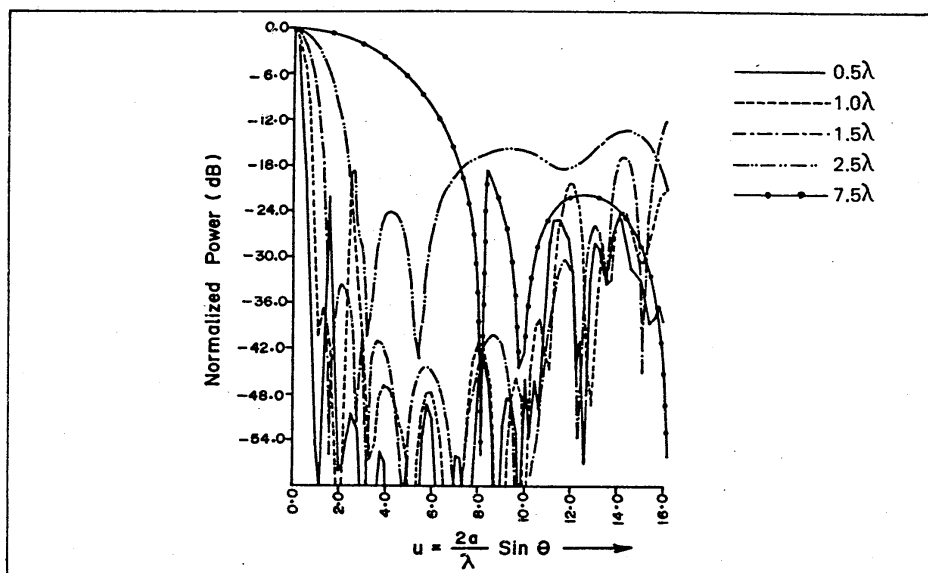


Figure 3. Vertical power pattern in the  $\phi = 0^\circ$  plane for shaded ( $-20\text{dB}$ , side-lobe level) at different operating wavelengths.

For each  $F'(u)$  (shaded pattern for  $-20\text{dB}$  side-lobe level), different selected numbers of iterations at various operating wavelengths are given in Table 1.

From figure 3, it can be noted that the suppressed side-lobe levels of the power pattern up to operating wavelengths ( $0.5\lambda$ ,  $1.0\lambda$ ,  $1.5\lambda$  and  $7.5\lambda$ ) are satisfactorily suppressed (below  $-20\text{dB}$ ). The power pattern of the operating wavelength  $2.5\lambda$  is not shaded below  $-20\text{dB}$ . For an operating wavelength of  $2.5\lambda$ , the maximum far-out side-lobe level degrades up to  $-16\text{dB}$  at  $u = 9.0$  and  $-14\text{dB}$  at  $u = 15.0$ . The existence of the above side-lobes, which are less in number, lying in the far-out region, cannot affect the performance of the main beam and can still be useful for bathymetric purposes.

In order to obtain the excitation coefficients across the radiators on each circle for the above shaded pattern, an inverse technique is applied at different operating wavelengths. The excitation level can be rewritten as

$$G(t) = 2/\pi^2 \sum_{q=0}^{q-1} \frac{F'(u_q) \cdot J_0(u_q t)}{J_0^2(u_q \pi)} \quad (3)$$

where  $F'(u_q)$ , the values of side-lobe maxima from eqn.3 for corresponding  $u_q (= 2a \sin \theta_q)$ , and  $t = a_n/a$ ,  $J_0(u_q \pi)$  and  $J_0(u_q t)$  are related Bessel functions of corresponding arguments for  $u_q \pi$  and  $u_q t$  respectively.

The values of the excitation coefficients at different operating wavelengths with respect to different radii  $a_n$  are shown in Table 2. The above inverse technique was applied, with the patterns obtained as shown in Figure 3, and the consequent results are shown in Table 2. The values in Table 2 show moderate levels of amplitude across each radiator. The higher values of excitations, as well as negative values, which ultimately introduce the concept of less array sensitivity, of less practical interest, are not observed here.

Table 2  
Coefficient of excitation of each array element for different radii at given operating wavelengths, for the shaded (-20dB) array.

	Operating wavelengths $\lambda$	$t = a_n/a$	G(t)
1	0.5	.50 $\pi$	.137
		.75 $\pi$	.181
		1.00 $\pi$	.143
2	1.0	.50 $\pi$	.098
		.75 $\pi$	.182
		1.00 $\pi$	.242
3	1.5	.50 $\pi$	1.000
		.75 $\pi$	.086
		1.00 $\pi$	.216
4	2.5	.50 $\pi$	.039
		.75 $\pi$	.192
		1.00 $\pi$	.220
5	7.5	.50 $\pi$	.229
		.75 $\pi$	.159
		1.00 $\pi$	.209

Table 3.  
Calculated values of Noise Improvement Figure

	Operating wavelength $\lambda$	$f/f_o^*$	NIF (point source radiators)	NIF (unshaded pattern)	NIF (shaded pattern -20dB)
1	0.5 (60kHz)	2.0	7.0	31.0	47.0
2	1.0 (30kHz)	1.0	6.0	14.0	30.0
3	1.5 (20kHz)	.66	6.0	9.0	16.0
4	2.5 (12kHz)	.40	6.0	7.0	11.0
5	7.5 (4kHz)	.133	13.0	13.0	16.0

Metzger [6] developed a method to calculate the noise improvement figure for spherically isotropic noise, to estimate the performance obtained from beam-forming and to compare the beam-forming methods. In order to study the noise improvement figure for power patterns with and without the shaded pattern, the following calculation was carried out. The noise improvement figure (NIF) for spherical modelled noise for the  $\phi = 0^\circ$  plane can be given as [6]

$$NIF = 1 / \int_0^{\pi/2} F(\theta, \phi) \sin\theta d\theta \quad , \quad (4)$$

where  $F(\theta, \phi)$  is shaded on unshaded beam-patterns. This is an approximation of the generalised form of the NIF for spherically isotropic modelled noise.

Table 3 gives the comparative analysis of NIF for point source radiators as well as circular disk radiators for shaded and unshaded patterns. The above comparison was made to observe the effect of array pattern changes in unshaded and shaded arrays of circular disk elements with ideal coaxial circular array factors assuming each element is a point source, i.e., the element pattern in eqn.1 is equivalent to unity.

Table 3 shows the highest values of NIF at the operating wavelength  $0.5\lambda$ , and it is also shown that NIF for the -20dB shaded power pattern and the uniformly excited power pattern for distance radiators decreases up to  $2.5\lambda$ , increasing again at  $7.5\lambda$ . The

NIF for the uniformly excited point source radiators of the coaxial circular array, show constancy at  $1.0\lambda$ ,  $1.5\lambda$ ,  $2.5\lambda$ , and a maximum value at  $7.5\lambda$ .

In general, the higher values of NIF for the spherical noise model show a good capability of such an array structure to reject noise from the sea environment. Higher values of NIF obtained for a shaded pattern established the suitability of such types of shading technique.

### Conclusions

Side-lobe suppressed power patterns ( $-20\text{dB}$ ) are plotted for a coaxial circular array at different operating wavelengths, which indicates the suitability of such an array geometry for very narrow main-beam angles and better coverages. Moderate values of excitation level found for each radiator established that the sensitivity of array element will not degrade.

The highest noise improvement figure (NIF) for the shaded patterns shows the effectiveness of side-lobe suppressed beam-patterns for the elimination of sea environment noise at different operating wavelengths.

### Acknowledgements

The author acknowledges the help of T. Sudhakar and T. Ramprasad, Scientists, NIO, during the present work. Thanks are due to Miss Alison Luis for typing the manuscript.

### References

- [1] V.H. Rumsey, *Frequency Independent Antenna*, *Inst. Radio Eng. Nat. Convention Rec. Part 1, 5*, 114-119 (1957).
- [2] B. Chakraborty, *Coaxial circular array - study of far-field pattern and field frequency responses*, *J. Acoust. Soc. Am.* 79, 4, 1161-1163, (1986).
- [3] T.T. Taylor, *Design of circular apertures for narrow beamwidth and low side-lobes*, *IRE Trans. on Antenna Propagation*, AP8, 1, 17-22, (1960).
- [4] R.C. Hansen, *Tables of Taylor distribution for circular aperture antenna*, *IRE Trans. on Antenna Propagation*, AP8, 1, 23-26, (1960).
- [5] R.S. Elliot, *Antenna Theory and Design*, Prentice Hall, pp 216-217, (1985).
- [6] Metzger, D.K.Jr., *Signal processing equipment and techniques for use in measuring ocean acoustic multipath structures*, Ph.D. Thesis, p.151, submitted to the Univ of Michigan, (1983).

(Received 13 February 1987 and in revised form 21 July 1987)